

UC Berkeley

UC Berkeley Previously Published Works

Title

The vitamin D receptor as a potential target for the toxic effects of per- and polyfluoroalkyl substances (PFASs): An in-silico study.

Permalink

<https://escholarship.org/uc/item/65k8h3b9>

Authors

Azhagiya Singam, Ettayapuram

Smith, Martyn

Wang, Jen Chywan

et al.

Publication Date

2023-01-15

DOI

10.1016/j.envres.2022.114832

Peer reviewed



HHS Public Access

Author manuscript

Environ Res. Author manuscript; available in PMC 2024 January 15.

Published in final edited form as:

Environ Res. 2023 January 15; 217: 114832. doi:10.1016/j.envres.2022.114832.

The vitamin D receptor as a potential target for the toxic effects of per- and polyfluoroalkyl substances (PFASs): An in-silico study

Ettayapuram Ramaprasad Azhagiya Singam¹, Kathleen A. Durkin^{1,*}, Michele A. La Merrill², J. David Furlow³, Jen-Chywan Wang⁴, Martyn T. Smith^{5,*}

¹Molecular Graphics and Computation Facility, College of Chemistry, University of California, Berkeley, CA 94720, USA

²Department of Environmental Toxicology, University of California, Davis, CA 95616, USA

³Department of Neurobiology, Physiology and Behavior, University of California, Davis 95616, CA, USA

⁴Department of Nutritional Sciences and Toxicology, University of California, Berkeley, CA 94720, USA

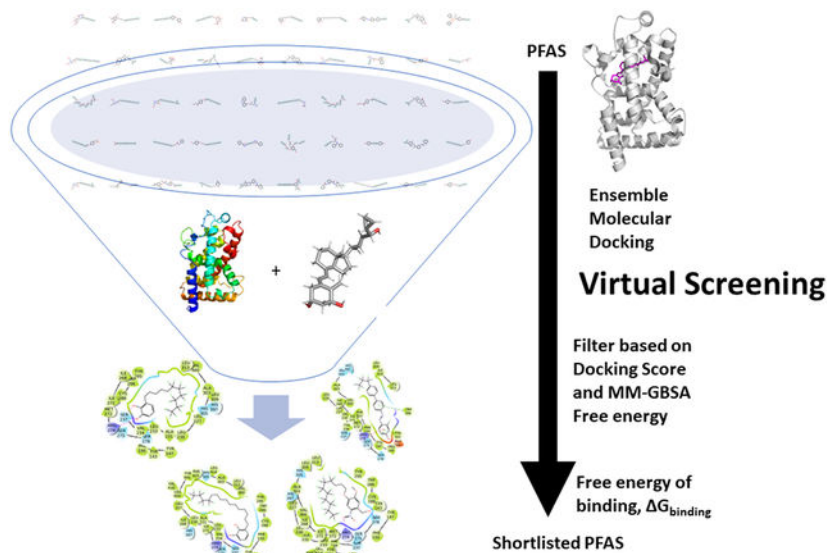
⁵Division of Environmental Health Sciences, School of Public Health, University of California Berkeley, CA 94720, USA

Abstract

Due to their persistence and toxicity, perfluoroalkyl and polyfluoroalkyl substances (PFASs) constitute significant hazards to human health and the environment. Their effects include immune suppression, altered hormone levels, and osteoporosis. Recently, the most studied PFAS, perfluorooctanoic acid (PFOA), was shown to competitively binding to the Vitamin D receptor (VDR). VDR plays a crucial role in regulating genes involved in maintaining immune, endocrine, and calcium homeostasis, suggesting it may be a target for at least some of the health effects of PFAS. Hence, in this study, the potential binding of 5,206 PFASs to VDR was examined using molecular docking, molecular dynamics, and free energy binding calculations. We identified 14 PFAS that are predicted to interact strongly with VDR, similar to the natural ligands. We further investigated the interactions of VDR with 256 PFASs of established commercial importance. Eighty-three (32%) of these 256 commercially important PFAS were predicted to be stronger binders to VDR than PFOA. At least 16 PFASs of regulatory importance, because they have been identified in water supplies and human blood samples, were also more potent binders to VDR than PFOA. Further, PFASs are usually found together in contaminated drinking water and human blood samples, which raises the concern that multiple PFASs may act together as a mixture on VDR function, potentially producing harmful effects on the immune, endocrine, and bone homeostasis.

Graphical Abstract

* Correspondence: To whom correspondence should be addressed. K. Durkin: Tel: +1(510) 642-6719; durkin@berkeley.edu ; M.T. Smith: Tel: (510) 642-8770; martynts@berkeley.edu.



Keywords

VDR; PFAS; Molecular Docking; Virtual Screening; Vitamin D3; Calcitriol; Bone; Immune; Endocrine disruption

1. Introduction

PFASs are synthetic chemicals used in consumer products such as clothing, furniture, etc. (Guelfo et al., 2021; Marchiandi et al., 2020). PFASs have been detected in groundwater (Sunderland et al., 2019), dust (Hall et al., 2020), and edible fish (Fair et al., 2019). The persistence of PFASs in the environment leads to exposure and accumulation in the human body over time (Ao et al., 2019; Brendel et al., 2018; Pelch et al., 2019; Seo et al., 2018; Sunderland et al., 2019). Previous studies have shown that PFASs cause a variety of harmful effects, including immunosuppression (Corsini et al., 2012; Lau et al., 2007; Shane et al., 2020), lowered bone mineral density (Khalil et al., 2016) and endocrine disruption of several systems including altered thyroid hormone and androgen levels (Ballesteros et al., 2017; Chambers et al., 2021) The mechanisms by which they produce these adverse effects remain unclear, however.

The most widely studied PFAS is PFOA. PFOA is immunotoxic (Liang et al., 2022) and may impair bone accrual and strength (Buckley et al., 2021). Recent evidence from *in silico* and *in vitro* studies showed that PFOA binds to the vitamin D receptor (VDR) and changes the activity of vitamin D-responsive genes (Di Nisio et al., 2020). VDR is a nuclear receptor family member. It mediates pleiotropic biological actions that include humoral and cellular immunity, bone formation and homeostasis, dietary calcium absorption, and androgen synthesis, wherein the VDR transcriptionally regulates the expression of genes involved in these complex processes. The natural ligand is 1,25-dihydroxy vitamin D3 (calcitriol), which binds to VDR and regulates gene expression related to calcium metabolism and homeostasis (Veldurthy et al., 2016) as well as other metabolic pathways. The circulating form of vitamin

D3 is 25-dihydroxy vitamin D3, also known as calcifediol. Disrupted Vitamin D synthesis or action has been shown to lead to adverse outcomes such as osteoporosis, Rickett's disease, and immune disorders (DeLuca, 2016; Mungai et al., 2021).

Given the importance of VDR in maintaining health, it is a potential target for PFAS binding, which may produce harmful effects. There is evidence that at least one legacy PFAS, namely PFOA, can interact with VDR. Here, we utilized *in silico* molecular docking, molecular dynamics, and free energy simulation to identify the subset of PFASs from the 5,206 PFASs listed on the Environmental Protection Agencies CompTox Dashboard in 2019 that potentially have a high affinity to bind to and impact VDR function. We compare their potential potency to that of PFOA.

2. Materials and methods

2.1. Receptor Preparation and Molecular Docking of Known Ligands

Molecular docking helps explore the nature of the interactions between a protein and a ligand. To validate a molecular docking protocol for human VDR, we docked 13 known ligands: the endogenous ligand 1,25-dihydroxy vitamin D3 (calcitriol) and its known synthetic and natural analogs (alfacalcidol, calcipotriol, eldecalcitol, inecalcitol, tacalcitol, calcidiol, ergocalciferol, paricalcitol, calciferol, doxercalciferol, falecalcitriol, and seocalcitol) using the Glide docking program (Maestro et al., 2019) to an ensemble of different VDR conformations of the ligand binding domain (LBD). Molecular docking considers the protein a rigid entity, while ligands can move flexibly relative to the receptor's binding site. However, since different ligands can induce different receptor conformations *in vivo*, it is difficult for docking methods to predict the binding poses of different ligands when using only a single conformation of the receptor. Ensemble docking helps tackle this problem by screening a ligand library against an array of multiple rigid receptor conformations. Hence, in this study, three individual representative structures of the LBD of wild-type VDR were obtained from the Protein Data Bank (PDB ID: 2HAM, 1DB1, and 3AUR) and were prepared using the protein preparation wizard protocol in the Maestro software suite (Schrödinger; 2018–4). This process adds hydrogen atoms, assigns partial atomic charges to the protein, and minimizes the overall energy using an OPLS3e force field (Harder et al., 2016) with default parameters. Then, using Glide, a docking grid for each of the ensemble VDR LBD conformations was created by selecting the centroid of the co-crystallized ligand.

2.2 Ligand Preparation and Molecular Docking of PFAS to VDR

Chemicals structures of PFASs were downloaded on 15th October 2019 at 12:58 PM from the EPA (Environmental Protection Agency, USA) CompTox Chemicals Dashboard (<https://comptox.epa.gov/dashboard>). The date of download is noted because the Dashboard is regularly updated. Those PFAS chemicals without SMILES codes were removed from the downloaded dataset. The 5,206 PFASs remaining were then prepared using Schrodinger's (Release, 2019) LigPrep module by generating ionization, tautomeric states, and stereoisomers at pH 7.4, with a maximum of 32 states for each PFAS chemical. Each PFAS tautomer, ionization variant, and stereoisomer state was treated as a unique structure

which was then energy minimized using the optimized potentials for liquid simulations (OPLS3e) force field with default parameters. A total of 9129 PFAS states were minimized and then docked to the wild-type VDR ensemble conformations using the Glide XP algorithm (Friesner et al., 2006, 2004; Halgren et al., 2004). We combined the docking results from the multiple VDR conformations and ligand charge states by keeping the top-ranking PFAS chemicals based on their docking scores. Those PFASs with a docking score ≤ -12 were shortlisted for further investigation by molecular dynamics simulation. This cutoff was based on the previously calculated docking scores of the known ligands.

2.3 Molecular Dynamics (MD) Simulation

MD simulations were performed using Desmond 3.2 with the OPLS3e force field. These simulations were done for each of the VDR + known ligand complexes and VDR + PFAS complexes, which had been shortlisted from the docking simulation. Each of the complexes was solvated using a TIP3P water model in an orthorhombic box with dimensions of $10 \text{ \AA} \times 10 \text{ \AA} \times 10 \text{ \AA}$ as buffer distances around the VDR + ligand complex with periodic boundary conditions. The total charge of the system was neutralized by adding counterions, and the solvent was set to a salt concentration of 0.15 M NaCl. After solvation, minimization and relaxation steps on the solvated complex were performed using Desmond with default parameters. Data production runs were performed on each VDR + ligand complex (for known ligands and shortlisted PFASs) for 50 nanoseconds using a two femtosecond time step to integrate the equations of motion in the NPT ensemble at 300 K and one atmospheric pressure, controlled by Nose-Hoover thermostat algorithm and Martyna-Tobias-Klein Barostat algorithm. The trajectories were saved every 50 ps for 1000 frames for each simulation.

2.4 Alchemical Free Energy Calculations using YANK

Absolute alchemical free energies were calculated for the shortlisted PFASs complexed with wild-type VDRs and known ligands with wild-type VDR using the YANK GPU-accelerated free energy calculation package (<https://github.com/choderalab/yank>). (Chodera and Shirts, 2011; Eastman et al., 2013; Eastman and Pande, 2015, 2010a, 2010b; Friedrichs et al., 2009; Shirts et al., 2007; Shirts and Chodera, 2008) The YANK protocol consisted of several steps: 1) The molecules (both protein and ligand) were each processed through LEaP (Case et al., 2021) to add appropriate hydrogen settings for the force field. 2) The shortlisted PFASs were parameterized using Antechamber (Wang et al., 2006) using the GAFF force field (Wang et al., 2004), and the partial atomic charges for each shortlisted PFAS were calculated using the AM1-BCC method (Jakalian et al., 2000). The AMBER FF14SB force field (Tian et al., 2020) was used for the VDRs. Each VDR + ligand complex was automatically solvated using the TIP3P water model in LEaP, and counter ions were added to neutralize the overall charge of the systems. The ligands were harmonically restrained with an automatically determined force constant to keep the ligand from diffusing away from the protein while in a weakly coupled state. Specifically, the restraint was applied so that the ligand was centered on the active site residues (residues F422, V418, Y401, L404, H305, L227, A303, L230, A231, L309, V300, L233, V234, Y295, W286, C288, F150, S237, Y143, Y147, S278, S275, R274, M272, I271, L313, I268, H397, L414, V418). The particle mesh Ewald (PME) summation with default parameters and a cutoff value of 9 \AA was used to calculate

the full-system periodic electrostatic interactions. The entire system was minimized using the L-BFGS algorithm implemented in OpenMM (Eastman et al., 2017). The production alchemical Hamiltonian exchange free energy calculations were carried out at 300 K and 1 atm using a Langevin integrator with a 2 fs timestep, 5.0 ps⁻¹ collision rate, and a molecular-scaling Monte Carlo barostat. YANK with OpenMMTools was used to run the simulations and each production simulation was carried out for 10000 iterations with 500 timesteps per iteration. The YANK auto protocol trailblazing feature was used for determining the alchemical pathway for each VDR + ligand complex. Using the Gibbs sampling scheme, a Hamiltonian replica exchange simulation was performed for each iteration to mix replicas. This process was repeated for each solvent simulation. Finally, absolute binding free energy (ΔG) of binding was estimated for each VDR + ligand complex using multistate Bennett acceptance ratio (MBAR) to get the minimally biased free energy estimate across the two phases. Extending the simulation to 20000 steps did not change the ΔG of binding and thus we judged these as equilibrated. The input script and other code for the alchemical free energy calculation analysis are given in the Supporting Information.

2.5 Single point MM-GBSA Free energy Calculation

We also calculated the MM-GBSA (Kollman et al., 2000; Srinivasan et al., 1998) single point free energy of binding using the AMBER 18 (Case et al., 2021) package for each of the shortlisted docked VDR + PFAS complexes. Partial atomic charges for the ligands were calculated utilizing Antechamber employing the AM1-BCC method (Jakalian et al., 2000), whereas the AMBER FF14SB force field was used for the protein. Each VDR + PFAS complex was solvated using a TIP3P water box. The solvated complexes were energy minimized in four steps: 1) Minimization relaxing the solute with a restraint weight of 500 kcal/mol/Å² for 1000 steps, 2) Minimization relaxing the solute with a restraint weight of 100 kcal/mol/Å² for 1000 steps, 3) Minimization relaxing the solute with a restraint weight of 1 kcal/mol/Å² for 1000 steps, and 4) 2500 steps of steepest descent without any positional restraint. The MM-GBSA binding free energy (ΔG_{bind}) of the minimized complex structure was then calculated using an infinite cutoff (999 Å) and a protein's dielectric constant of 4.

3. Results and Discussion

3.1. Docking of Known Ligands

Before screening the PFAS library of 5,206 compounds, we first validated the molecular docking protocol by docking a series of known ligands to LBD of human wild-type VDR. The binding pose of the calcipotriol and seocalcitol from the docking protocol was compared with that of co-crystallized calcipotriol (PDB ID: 1S19, resolution 2.10 Å) and seocalcitol (PDB ID: 1S0Z, resolution 2.40 Å). The superimposed binding poses obtained from docking versus the co-crystallized poses for calcipotriol and seocalcitol are given in Figure 1. For calcipotriol, the docking pose was similar to the X-ray crystal structure with a root mean square deviation (RMSD) of 0.47 Å. The RMSD between the docked pose of seocalcitol and the X-ray crystal structure was 1.78 Å which is within expected variation for a flexible molecule with common X-ray structure resolution. The docking protocol placed these known ligands within the binding pocket with a correct global orientation and thus confirmed that the parameters for docking small molecules to

VDR are suitable for reproducing the known experimental binding poses. We also docked other known ligands: alfacalcidol, eldecalcitol, inecalcitol, tacalcitol, calcidiol, calcitriol, ergocalciferol, paricalcitol, calciferol, doxercalciferol, and falecalcitriol, using the same docking parameters. The 2D ligand interaction diagrams for these ligands with their docking scores (Table 1) are given in Figure 2. All known ligands were bound in the ligand-binding pocket formed by residues: F422, V418, Y401, L404, H305, L227, A303, L230, A231, L309, V300, L233, V234, Y295, W286, C288, F150, S237, Y143, Y147, S278, S275, R274, M272, I271, L313, I268, H397, L414, V418. The known ligands form hydrogen bonds with Y143, H305, H397, R274, and S237. The docking scores for the known ligands docked to VDR ranged from -11.81 to -16.13 (Table 1), indicating strong binding. Molecular dynamics (MD) simulations were performed for 50 ns to analyze the stability of each of these VDR + known ligand complexes. RMSD plots of all the complexes are given in Supporting Information Figure S1. The figure shows that the RMSD values of alpha-carbons for different VDR + known ligand complexes fluctuate as expected around their average during the MD simulation. The interaction fraction of VDR + known ligand contact is given in Figure 3. The hydrogen bonds between the known ligands and VDR (Y143, H305, H397, R274, and S237) have the highest time occupancy, and this result is in agreement with the previous literature (Tocchini-Valentini et al., 2004). The calculated alchemical binding free energies (G_{bind}) computed using YANK, for all the known ligands are given in Table 1. Calcidiol has the least negative predicted binding affinity with the calculated free energy of binding of -19.404 ± 0.43 kcal/mol, whereas calcipotriol (is calculated to) bind to VDR with the highest affinity ($G_{\text{bind}} = -33.171 \pm 0.2$).

3.2 Virtual Screening of over 5,000 PFASs against VDR

The virtual screening of PFASs against VDR was performed using molecular docking and molecular dynamics simulation techniques. The docking scores for all 5,206 PFASs with VDR are given in Supporting Information Table S2. Different PFAS classes (Su and Rajan, 2021) of the screened library is given in Supporting information Figure S2 and S3. Initially, we shortlisted the PFAS chemicals with a docking score ≤ -12 since the minimum docking score for a known ligand is -11.81 . Fourteen PFASs had docking scores more negative than any known ligands, showing a high potential for interaction with VDR (Table 2). The 2D interaction diagram of the top-scoring PFASs with VDR is shown in Figure 4. The interaction fraction of contact from our MD simulations shows that the hydrophobic interaction between the PFASs and VDR is similar to that of known ligands (Figure 5). The top PFASs also formed hydrogen bonds with Y143, R274, and S237. The root-mean-square fluctuation (RMSF) of the $\text{C}\alpha$ atom was calculated for each residue of the complexes of VDR + known ligands or VDR + PFASs, to understand how the different ligands induce flexibility in the VDR (Figure 6). Similar RMSFs was observed for all VDR complexes, with both the known ligands and the PFASs. Interestingly, a recent study showed that PFOA induces a similar change in the RMSF in the ligand-binding domain of VDR (Di Nisio et al., 2020). Due to the computational cost, the Alchemical binding free energies for only 11 of the shortlisted PFAS were calculated. The calculated G_{bind} data are summarized in Table 2. The G_{bind} values for 6 PFAS (DTXSID20897499, DTXSID30896731, DTXSID40896227, DTXSID40897496, DTXSID60895974, and DTXSID70895980) were more negative than -20 kcal/mol suggesting that these chemicals strongly bind to VDR, and thus we classified

these as strong binders. DTXSID10896537, DTXSID40881032, DTXSID50858139 showed weaker binding to VDR with a G_{bind} more positive (in the range of -3 to -10 kcal/mol). DTXSID80827555 and DTXSID90785778 had the G_{bind} of -16.122 ± 0.437 kcal/mol and -17.701 ± 0.198 kcal/mol, respectively, and these chemicals were classified as moderate binders. The primary class of shortlisted PFAS belongs to chemicals containing side-chain aromatics, with steroid-backbone and extended aliphatic fluorocarbon sidechains being other common features.

3.3 Virtual screening results for commercially relevant PFASs

Recently, Buck and co-workers suggested that there are only 256 chemicals in the PFAS class that are highly commercially relevant globally (Buck et al., 2021). Further, recent studies showed that one of the commercially important chemicals, PFOA, competitively binds to VDR and inhibits the expression of vitamin D responsive genes (Di Nisio et al., 2020). Di Nisio et al showed that the docking free energy for the PFOA using Autodock Vina was -9 kcal/mol, which is relatively weak compared to that of native ligand (1,25-dihydroxyvitamin D). The docking score and the single-point MM-GBSA free energy for PFOA and other commercially important PFASs, as calculated using our protocol. The docking score for PFOA using Glide is -8.07 and we found that 82 chemicals out of the 256 commercially important PFASs had docking scores more negative than -8.07 . The MM-GBSA score for PFOA is -34.01 kcal/mol. Eighty-three of the PFASs that were shortlisted in Table 3 had docking scores more negative than -8.07 and MM-GBSA (G_{bind}) scores more negative than -34.01 kcal/mol. So they are also likely to interact with VDR. Indeed, these 83 commercially important PFASs are likely stronger or equal to PFOA in binding interactions with VDR.

Table 3 also shows that 16 PFASs of regulatory concern, because they have been detected in the environment and/or human blood, have docking scores suggesting stronger interactions with VDR than PFOA. For two of these 16 chemicals of regulatory concern, perfluorododecanoic acid (DTXSID8031861) and perfluorotridecanoic acid (DTXSID90868151), we also calculated the alchemical free energy. The mode of binding along with alchemical binding free energy (G_{bind}) for these compounds are shown in Figure 7. These results show that Perfluorotridecanoic acid likely binds more strongly than Perfluorododecanoic acid. However, both of these chemicals have binding interactions with VDR that are similar to known ligands. These results suggest that commercially important PFASs of regulatory concern can impact VDR function.

Due to the wide use of PFASs in consumer and industrial applications, and their observed persistence in the human body and the environment, these chemicals pose a human health concern. Here we have examined the potential of 5,206 PFASs to interact with and affect the function of VDR, a nuclear receptor that regulates the effects of vitamin D3 on the body, which includes the maintenance of bone strength and immune function. We found that 14 PFASs interact with VDR with equal or greater potency, and in a similar manner, to the natural ligand calcitriol and its analogs that are commonly found in vitamin D supplements. This was confirmed by molecular docking, molecular dynamics, and free energy calculations using MM-GBSA and alchemical approaches. These in silico results suggest that these

14 PFASs are likely to affect VDR function, which could cause osteoporosis or immune deficiency. The methodology used here does not predict agonism or antagonism but producing either high or low VDR activity may result in adverse outcomes. Confirmation of these data is needed in biological systems and should be a high priority.

We further examined the interactions of VDR with the 256 PFASs that were recently identified as being of significant commercial importance and compared them to the predicted interaction of PFOA with VDR since PFOA was recently shown to interact with VDR in experimental systems. We found that 82 (32%) of these 256 commercially important PFASs had docking and MM-GBSA scores that showed they were likely to be stronger or equal to PFOA in binding to VDR. We further showed that 16 of these PFASs were of high regulatory concern in addition to PFOA. These findings suggest that a third of commercially important PFASs plausibly affect VDR function as discussed and warrant further biological investigation. We also note that multiple PFASs are often found together in contaminated drinking water and human blood samples which raises the concern that multiple PFASs may act together as a mixture on VDR function, possibly amplifying their harmful effects.

3.4 The potential limitations of the study

The strengths of this study include a large number of PFASs (over 5,000) investigated and a focus on PFASs of commercial and regulatory importance. Further, the in-silico approach was calibrated and validated using known ligands of VDR and included molecular docking, molecular dynamics and free energy binding calculations using MM-GBSA and the computationally intensive alchemical approach. Although the current results show that our approach can be used to identify the potential binders of VDR successfully, a limitation is that we cannot evaluate the false-positive rate. Also, our binding results in VDR do not distinguish by agonism or antagonism activity, but we plan to explore this further as more experimental data become available. While these findings need to be experimentally validated in biological systems, they strongly suggest that many PFASs plausibly interact with VDR and may produce negative impacts on human health and the environment.

Conclusion

Computational modeling predicts that many PFASs of commercial and regulatory importance may impact the function of the vitamin D receptor and interfere with the beneficial effects of vitamin D₃. This may lead to increased osteoporosis and impaired immune function, two adverse effects that have been observed in epidemiological studies of humans exposed to PFASs. Biological validation of these in silico findings should be a high priority. These experimental approaches could include competition studies with native ligands and should include decoys and controls to provide data for an accurate estimate of the false positive rate.

Supplementary Material

Refer to Web version on PubMed Central for supplementary material.

ACKNOWLEDGEMENT

This study was supported by contracts from the Office of Environmental Health Hazard Assessment (OEHHA) of the California EPA (17-0023, 17-E0024) and USDA National Institute of Food and Agriculture, Hatch project 1002182 from the USDA National Institute of Food and Agriculture. The MGCF is funded by NIH S10OD023532 (to KAD).

References

- Ao J, Yuan T, Xia H, Ma Y, Shen Z, Shi R, Tian Y, Zhang J, Ding W, Gao L, Zhao X, Yu X, 2019. Characteristic and human exposure risk assessment of per- and polyfluoroalkyl substances: A study based on indoor dust and drinking water in China. *Environ. Pollut* 254, 112873. [PubMed: 31369910]
- Ballesteros V, Costa O, Iñiguez C, Fletcher T, Ballester F, Lopez-Espinosa M-J, 2017. Exposure to perfluoroalkyl substances and thyroid function in pregnant women and children: A systematic review of epidemiologic studies. *Environ. Int* 99, 15–28. [PubMed: 27884404]
- Brendel S, Fetter É, Staude C, Vierke L, Biegel-Engler A, 2018. Short-chain perfluoroalkyl acids: environmental concerns and a regulatory strategy under REACH. *Environ. Sci. Eur* 30. 10.1186/s12302-018-0134-4
- Buck RC, Korzeniowski SH, Laganis E, Adamsky F, 2021. Identification and classification of commercially relevant per- and poly-fluoroalkyl substances (PFAS). *Integr. Environ. Assess. Manag* 17, 1045–1055. [PubMed: 33991049]
- Buckley JP, Kuiper JR, Lanphear BP, Calafat AM, Cecil KM, Chen A, Xu Y, Yolton K, Kalkwarf HJ, Braun JM, 2021. Associations of maternal serum perfluoroalkyl substances concentrations with early adolescent bone mineral content and density: The health outcomes and measures of the environment (HOME) study. *Environ. Health Perspect* 129, 97011. [PubMed: 34585601]
- Case DA, Metin Aktulga H, Belfon K, Ben-Shalom I, Brozell SR, Cerutti DS, Cheatham TE III, Cruzeiro VWD, Darden TA, Duke RE, Giambasu G, Gilson MK, Gohlke H, Goetz AW, Harris R, Izadi S, Izmailov SA, Jin C, Kasavajhala K, Kaymak MC, King E, Kovalenko A, Kurtzman T, Lee T, LeGrand S, Li P, Lin C, Liu J, Luchko T, Luo R, Machado M, Man V, Manathunga M, Merz KM, Miao Y, Mikhailovskii O, Monard G, Nguyen H, O’Hearn KA, Onufriev A, Pan F, Pantano S, Qi R, Rahnamoun A, Roe DR, Roitberg A, Sagui C, Schott-Verdugo S, Shen J, Simmerling CL, Skrynnikov NR, Smith J, Swails J, Walker RC, Wang J, Wei H, Wolf RM, Wu X, Xue Y, York DM, Zhao S, Kollman PA, 2021. Amber 2021. University of California, San Francisco.
- Chambers WS, Hopkins JG, Richards SM, 2021. A review of per- and polyfluorinated alkyl substance impairment of reproduction. *Front Toxicol* 3, 732436. [PubMed: 35295153]
- Chodera JD, Shirts MR, 2011. Replica exchange and expanded ensemble simulations as Gibbs sampling: simple improvements for enhanced mixing. *J. Chem. Phys* 135, 194110. [PubMed: 22112069]
- Corsini E, Sangiovanni E, Avogadro A, Galbiati V, Viviani B, Marinovich M, Galli CL, Dell’Agli M, Germolec DR, 2012. In vitro characterization of the immunotoxic potential of several perfluorinated compounds (PFCs). *Toxicol. Appl. Pharmacol* 258, 248–255. [PubMed: 22119708]
- DeLuca HF, 2016. Vitamin D: Historical overview. *Vitam. Horm* 100, 1–20. [PubMed: 26827946]
- Di Nisio A, Rocca MS, De Toni L, Sabovic I, Guidolin D, Dall’Acqua S, Acquasaliente L, De Filippis V, Plebani M, Foresta C, 2020. Endocrine disruption of vitamin D activity by perfluoro-octanoic acid (PFOA). *Sci. Rep* 10, 16789. [PubMed: 33033332]
- Eastman P, Friedrichs MS, Chodera JD, Radmer RJ, Bruns CM, Ku JP, Beauchamp KA, Lane TJ, Wang L-P, Shukla D, Tye T, Houston M, Stich T, Klein C, Shirts MR, Pande VS, 2013. OpenMM 4: A reusable, extensible, hardware independent library for high performance molecular simulation. *J. Chem. Theory Comput* 9, 461–469. [PubMed: 23316124]
- Eastman P, Pande VS, 2015. OpenMM: A hardware independent framework for molecular simulations. *Comput. Sci. Eng* 12, 34–39. [PubMed: 26146490]
- Eastman P, Pande VS, 2010a. Efficient nonbonded interactions for molecular dynamics on a graphics processing unit. *J. Comput. Chem* 31, 1268–1272. [PubMed: 19847780]

- Eastman P, Pande VS, 2010b. CCMA: A robust, parallelizable constraint method for molecular simulations. *J. Chem. Theory Comput* 6, 434–437. [PubMed: 20563234]
- Eastman P, Swails J, Chodera JD, McGibbon RT, Zhao Y, Beauchamp KA, Wang L-P, Simmonett AC, Harrigan MP, Stern CD, Wiewiora RP, Brooks BR, Pande VS, 2017. OpenMM 7: Rapid development of high performance algorithms for molecular dynamics. *PLoS Comput. Biol* 13, e1005659. [PubMed: 28746339]
- Fair PA, Wolf B, White ND, Arnott SA, Kannan K, Karthikraj R, Vena JE, 2019. Perfluoroalkyl substances (PFASs) in edible fish species from Charleston Harbor and tributaries, South Carolina, United States: Exposure and risk assessment. *Environ. Res* 171, 266–277. [PubMed: 30703622]
- Friedrichs MS, Eastman P, Vaidyanathan V, Houston M, Legrand S, Beberg AL, Ensign DL, Bruns CM, Pande VS, 2009. Accelerating molecular dynamic simulation on graphics processing units. *J. Comput. Chem* 30, 864–872. [PubMed: 19191337]
- Friesner RA, Banks JL, Murphy RB, Halgren TA, Klicic JJ, Mainz DT, Repasky MP, Knoll EH, Shelley M, Perry JK, Shaw DE, Francis P, Shenkin PS, 2004. Glide: a new approach for rapid, accurate docking and scoring. 1. Method and assessment of docking accuracy. *J. Med. Chem* 47, 1739–1749. [PubMed: 15027865]
- Friesner RA, Murphy RB, Repasky MP, Frye LL, Greenwood JR, Halgren TA, Sanschagrin PC, Mainz DT, 2006. Extra precision glide: docking and scoring incorporating a model of hydrophobic enclosure for protein-ligand complexes. *J. Med. Chem* 49, 6177–6196. [PubMed: 17034125]
- Guelfo JL, Korzeniowski S, Mills MA, Anderson J, Anderson RH, Arblaster JA, Conder JM, Cousins IT, Dasu K, Henry BJ, Lee LS, Liu J, McKenzie ER, Willey J, 2021. Environmental sources, chemistry, fate, and transport of per- and polyfluoroalkyl substances: State of the science, key knowledge gaps, and recommendations presented at the August 2019 SETAC focus topic meeting. *Environ. Toxicol. Chem* 40, 3234–3260. [PubMed: 34325493]
- Halgren TA, Murphy RB, Friesner RA, Beard HS, Frye LL, Pollard WT, Banks JL, 2004. Glide: a new approach for rapid, accurate docking and scoring. 2. Enrichment factors in database screening. *J. Med. Chem* 47, 1750–1759. [PubMed: 15027866]
- Hall SM, Patton S, Petreas M, Zhang S, Phillips AL, Hoffman K, Stapleton HM, 2020. Per- and polyfluoroalkyl substances in dust collected from residential homes and fire stations in north America. *Environ. Sci. Technol* 54, 14558–14567. [PubMed: 33143410]
- Jakalian A, Bush BL, Jack DB, Bayly CI, 2000. Fast, efficient generation of high-quality atomic charges. AM1-BCC model: I. Method. *J. Comput. Chem* 21, 132.
- Khalil N, Chen A, Lee M, Czerwinski SA, Ebert JR, DeWitt JC, Kannan K, 2016. Association of perfluoroalkyl substances, bone mineral density, and osteoporosis in the U.s. population in NHANES 2009–2010. *Environ. Health Perspect* 124, 81–87. [PubMed: 26058082]
- Kollman PA, Massova I, Reyes C, Kuhn B, Huo S, Chong L, Lee M, Lee T, Duan Y, Wang W, Donini O, Cieplak P, Srinivasan J, Case DA, Cheatham TE 3rd, 2000. Calculating structures and free energies of complex molecules: combining molecular mechanics and continuum models. *Acc. Chem. Res* 33, 889–897. [PubMed: 11123888]
- Lau C, Anitole K, Hodes C, Lai D, Pfahles-Hutchens A, Seed J, 2007. Perfluoroalkyl acids: a review of monitoring and toxicological findings. *Toxicol. Sci* 99, 366–394. [PubMed: 17519394]
- Liang L, Pan Y, Bin L, Liu Y, Huang W, Li R, Lai KP, 2022. Immunotoxicity mechanisms of perfluorinated compounds PFOA and PFOS. *Chemosphere* 291, 132892. [PubMed: 34780734]
- Maestro MA, Molnár F, Carlberg C, 2019. Vitamin D and its synthetic analogs. *J. Med. Chem* 62, 6854–6875. [PubMed: 30916559]
- Marchiandi J, Green MP, Dagnino S, Anumol T, Clarke BO, 2020. Characterising the effects of per- and polyfluoroalkyl substances (PFASs) on health and disease: An opportunity for exposomics? *Curr. opin. environ. sci. health* 15, 39–48.
- Mungai LNW, Mohammed Z, Maina M, Anjumanara O, 2021. Vitamin D review: The low hanging fruit for human health. *J. Nutr. Metab* 2021, 6335681. [PubMed: 34900350]
- Pelch KE, Reade A, Wolffe TAM, Kwiatkowski CF, 2019. PFAS health effects database: Protocol for a systematic evidence map. *Environ. Int* 130, 104851. [PubMed: 31284092]
- Release S, 2019. 4: LigPrep. Schrödinger, LLC, New York, NY.

- Seo S-H, Son M-H, Choi S-D, Lee D-H, Chang Y-S, 2018. Influence of exposure to perfluoroalkyl substances (PFASs) on the Korean general population: 10-year trend and health effects. *Environ. Int* 113, 149–161. [PubMed: 29425899]
- Shane HL, Baur R, Lukomska E, Weatherly L, Anderson SE, 2020. Immunotoxicity and allergenic potential induced by topical application of perfluorooctanoic acid (PFOA) in a murine model. *Food Chem. Toxicol* 136, 111114. [PubMed: 31904477]
- Shirts MR, Chodera JD, 2008. Statistically optimal analysis of samples from multiple equilibrium states. *J. Chem. Phys* 129, 124105. [PubMed: 19045004]
- Shirts MR, Mobley DL, Chodera JD, Pande VS, 2007. Accurate and efficient corrections for missing dispersion interactions in molecular simulations. *J. Phys. Chem. B* 111, 13052–13063. [PubMed: 17949030]
- Srinivasan J, Miller J, Kollman PA, Case DA, 1998. Continuum solvent studies of the stability of RNA hairpin loops and helices. *J. Biomol. Struct. Dyn* 16, 671–682. [PubMed: 10052623]
- Su A, Rajan K, 2021. A database framework for rapid screening of structure-function relationships in PFAS chemistry. *Scientific Data* 8, 1–10. [PubMed: 33414438]
- Sunderland EM, Hu XC, Dassuncao C, Tokranov AK, Wagner CC, Allen JG, 2019. A review of the pathways of human exposure to poly- and perfluoroalkyl substances (PFASs) and present understanding of health effects. *J. Expo. Sci. Environ. Epidemiol* 29, 131–147. [PubMed: 30470793]
- Tian C, Kasavajhala K, Belfon KAA, Raguette L, Huang H, Miguez AN, Bickel J, Wang Y, Pincay J, Wu Q, Simmerling C, 2020. ff19SB: Amino-Acid-Specific Protein Backbone Parameters Trained against Quantum Mechanics Energy Surfaces in Solution. *J. Chem. Theory Comput* 16, 528–552. [PubMed: 31714766]
- Tocchini-Valentini G, Rochel N, Wurtz J-M, Moras D, 2004. Crystal structures of the vitamin D nuclear receptor liganded with the vitamin D side chain analogues calcipotriol and seocalcitol, receptor agonists of clinical importance. Insights into a structural basis for the switching of calcipotriol to a receptor antagonist by further side chain modification. *J. Med. Chem* 47, 1956–1961. [PubMed: 15055995]
- Veldurthy V, Wei R, Oz L, Dhawan P, Jeon YH, Christakos S, 2016. Vitamin D, calcium homeostasis and aging. *Bone Res.* 4, 16041. [PubMed: 27790378]
- Wang J, Wang W, Kollman PA, Case DA, 2006. Automatic atom type and bond type perception in molecular mechanical calculations. *J. Mol. Graph. Model* 25, 247–260. [PubMed: 16458552]
- Wang J, Wolf RM, Caldwell JW, Kollman PA, Case DA, 2004. Development and testing of a general amber force field. *J. Comput. Chem* 25, 1157–1174. [PubMed: 15116359]

Highlights

- 5,206 PFASs were evaluated by in silico methods for their potential to bind to Vitamin D receptor (VDR).
- 14 PFAS are predicted to strongly interact with VDR with a potency similar to the natural ligands.
- Eighty-three (32%) of 256 commercially important PFAS were predicted to be stronger binders than PFOA.

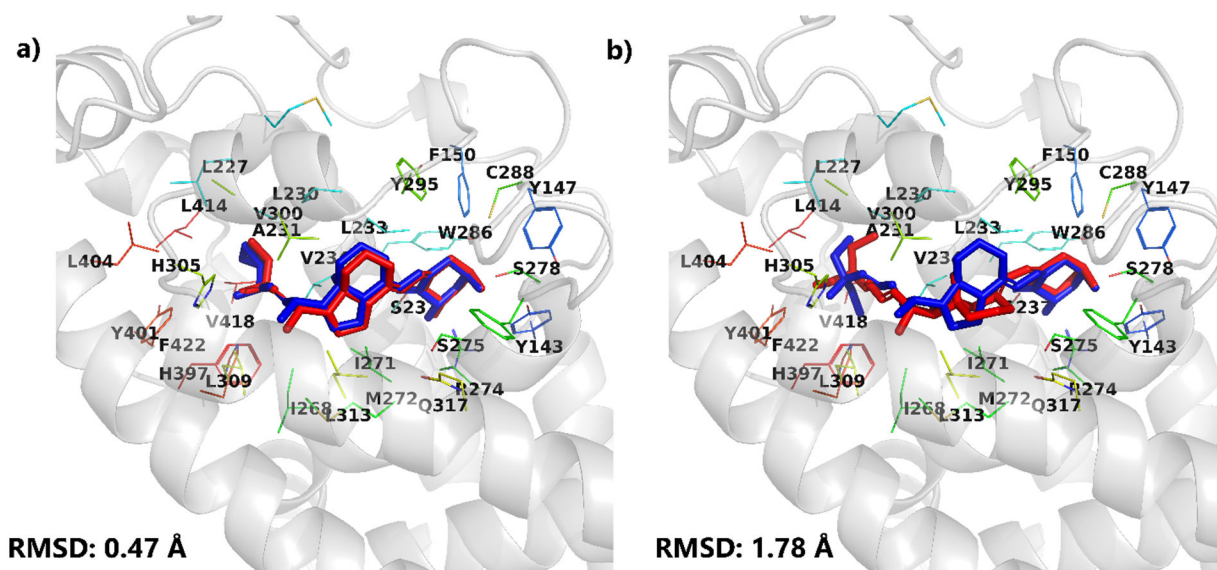


Figure 1.

A) Superimposed co-crystallized structures (red) (PDB: 1S19, 1S0Z) and docked binding pose (blue) of a) calcipotriol and b) seocalcitol. Hydrogen atoms are not shown for clarity.

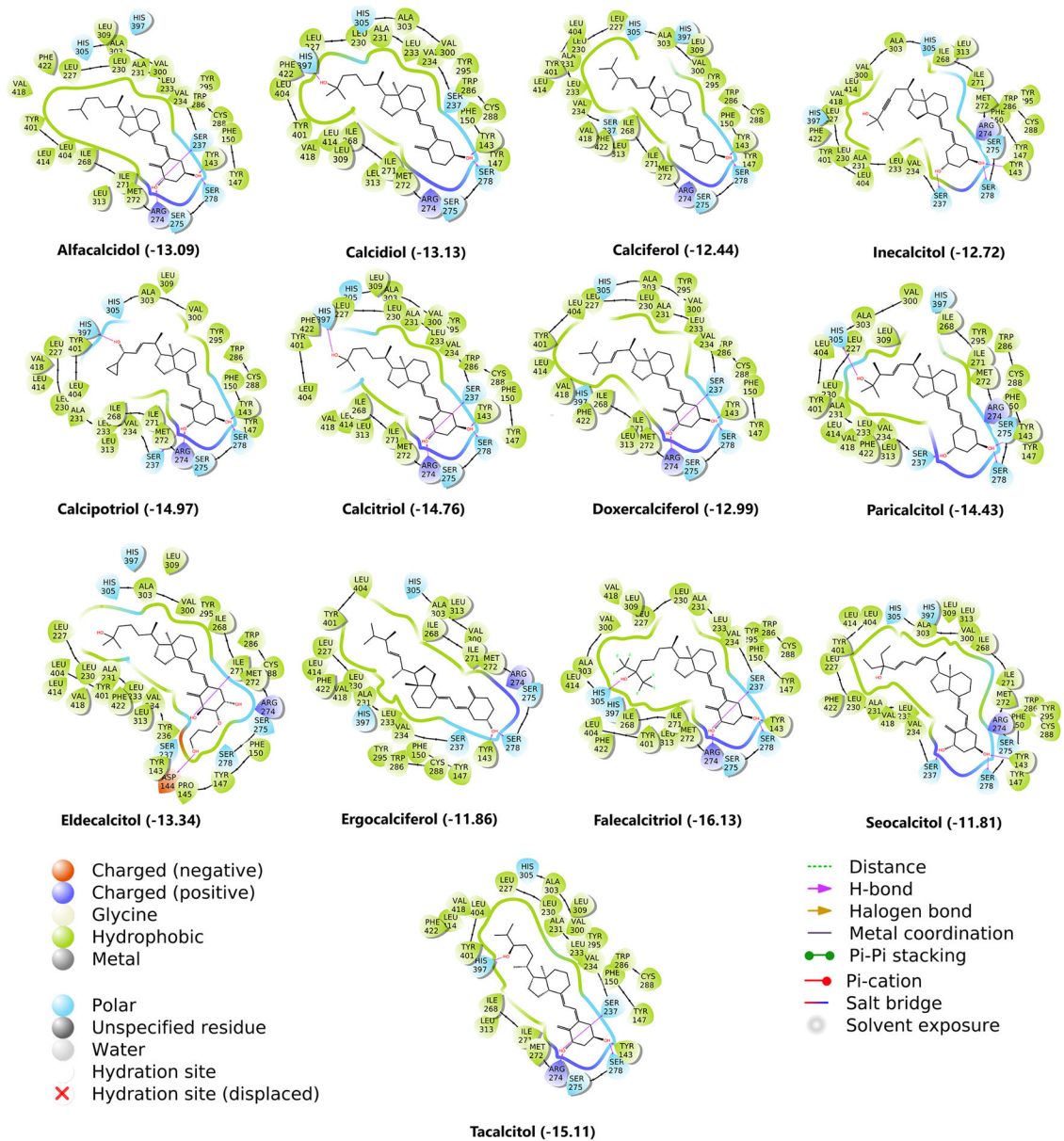


Figure 2. 2D interaction diagrams of calcitriol (1,25-dihydroxy vitamin D₃) and known analogs with wild type VDR. Docking scores (kcal/mol) are in brackets.

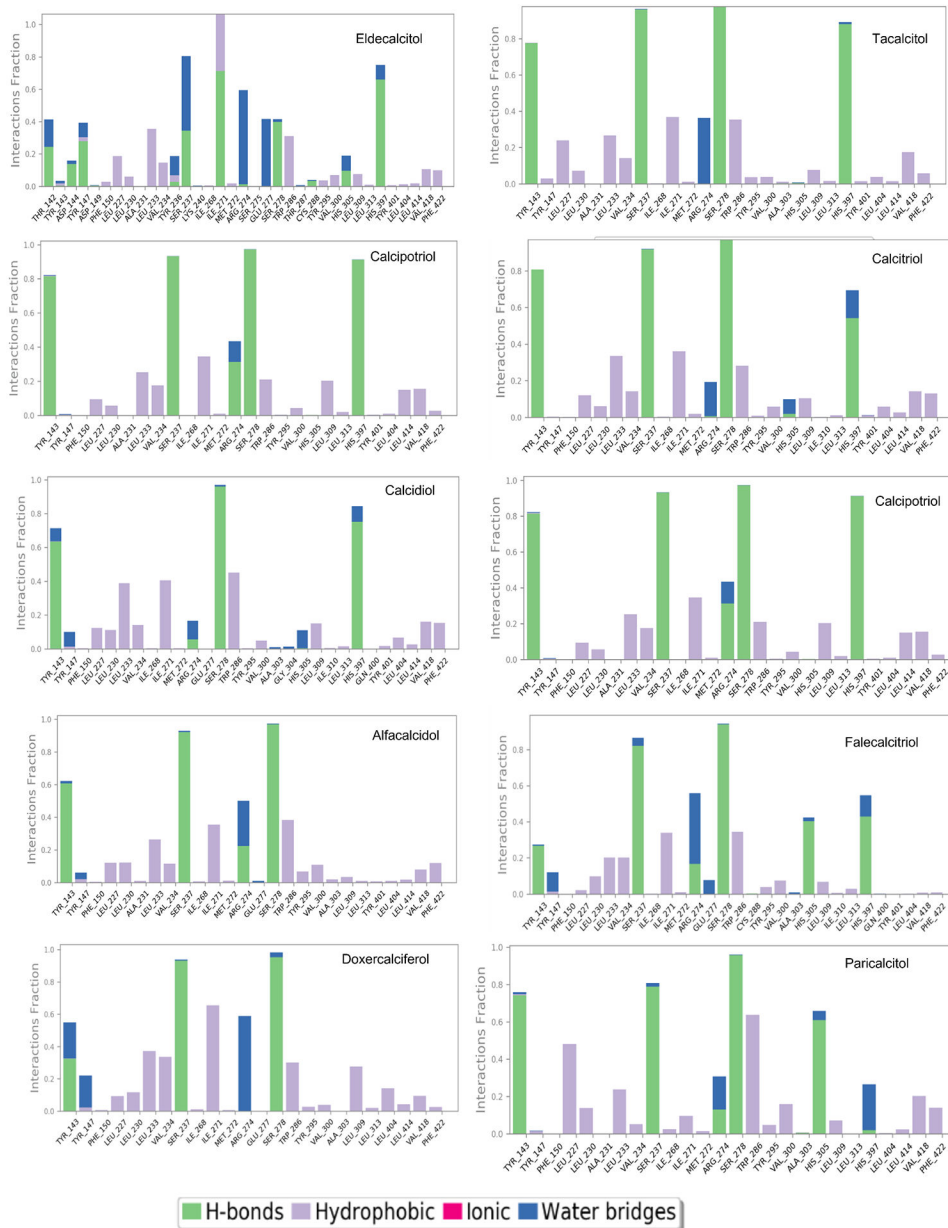


Figure 3. Interaction fraction of VDR + known ligand contacts during 50ns MD simulation.

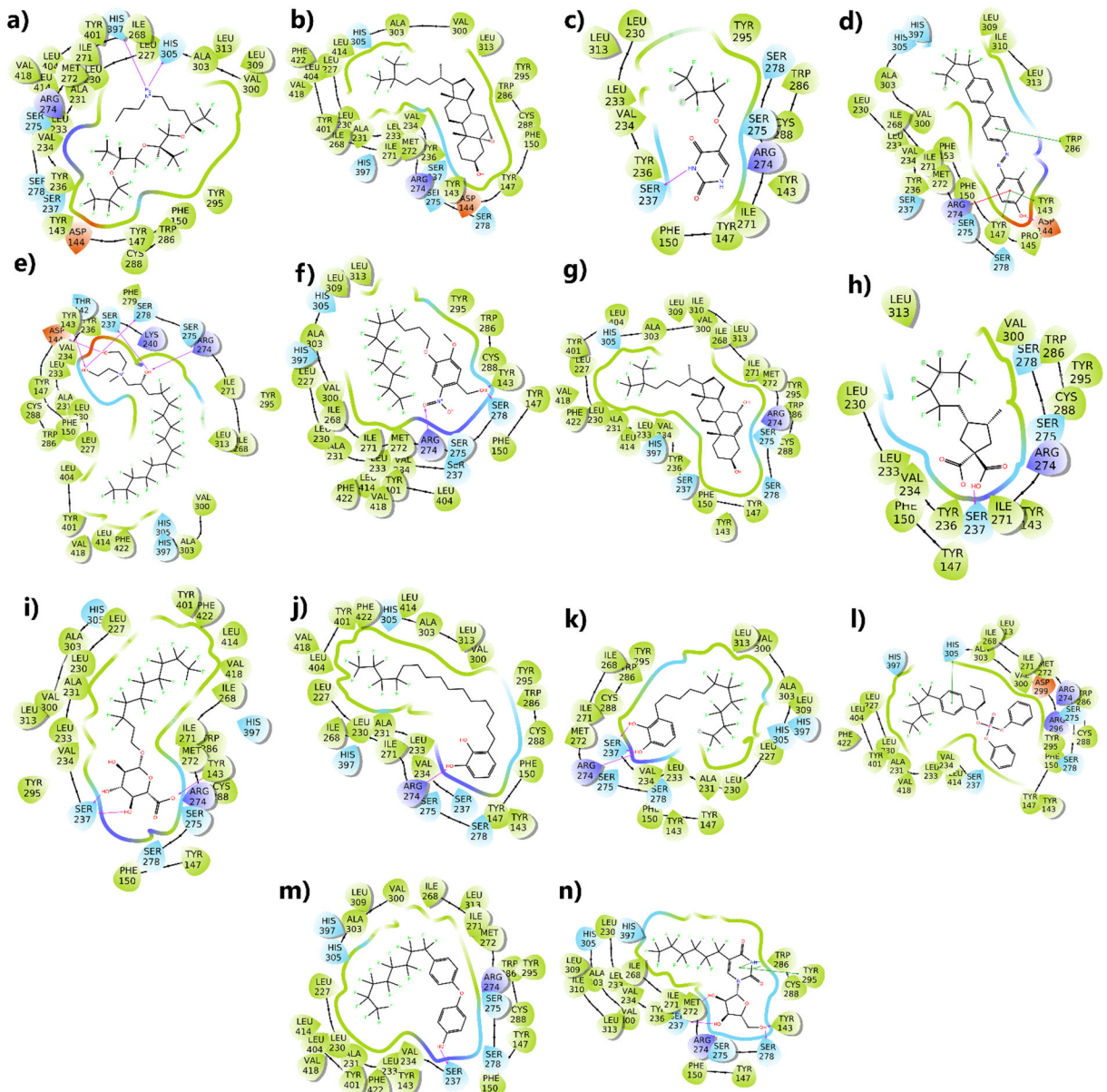


Figure 4.

2D interaction diagrams of VDR with 14 shortlisted PFAs a) DTXSID10896537, b) TXSID20897499, c) DTXSID30309992, d) DTXSID30896731, e) DTXSID40881032, f) DTXSID40896227, g) DTXSID40897496, h) DTXSID50379718, i) DTXSID50858139, j) DTXSID60895974, k) DTXSID70895980, l) DTXSID80827555, m) DTXSID90785778, and n) DTXSID90896292.

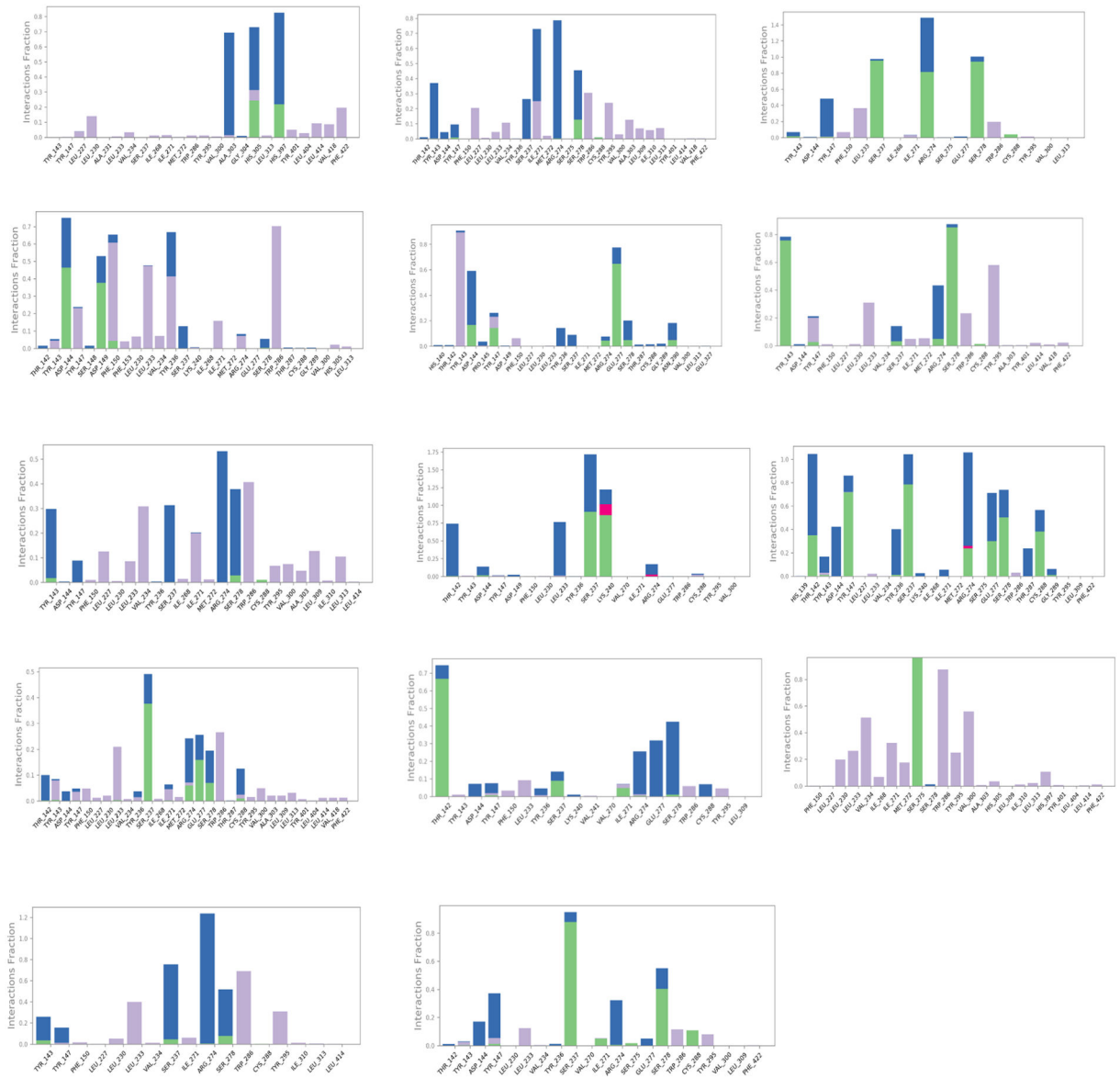


Figure 5: Interaction fraction of VDR + PFASs contacts during MD simulation a) DTXSID10896537, b) DTXSID20897499, c) DTXSID30309992, d) DTXSID30896731, e) DTXSID40881032, f) DTXSID40896227, g) DTXSID40897496, h) DTXSID50379718, i) DTXSID50858139, j) DTXSID60895974, k) DTXSID70895980, l) DTXSID80827555, m) DTXSID90785778, and n) DTXSID90896292.

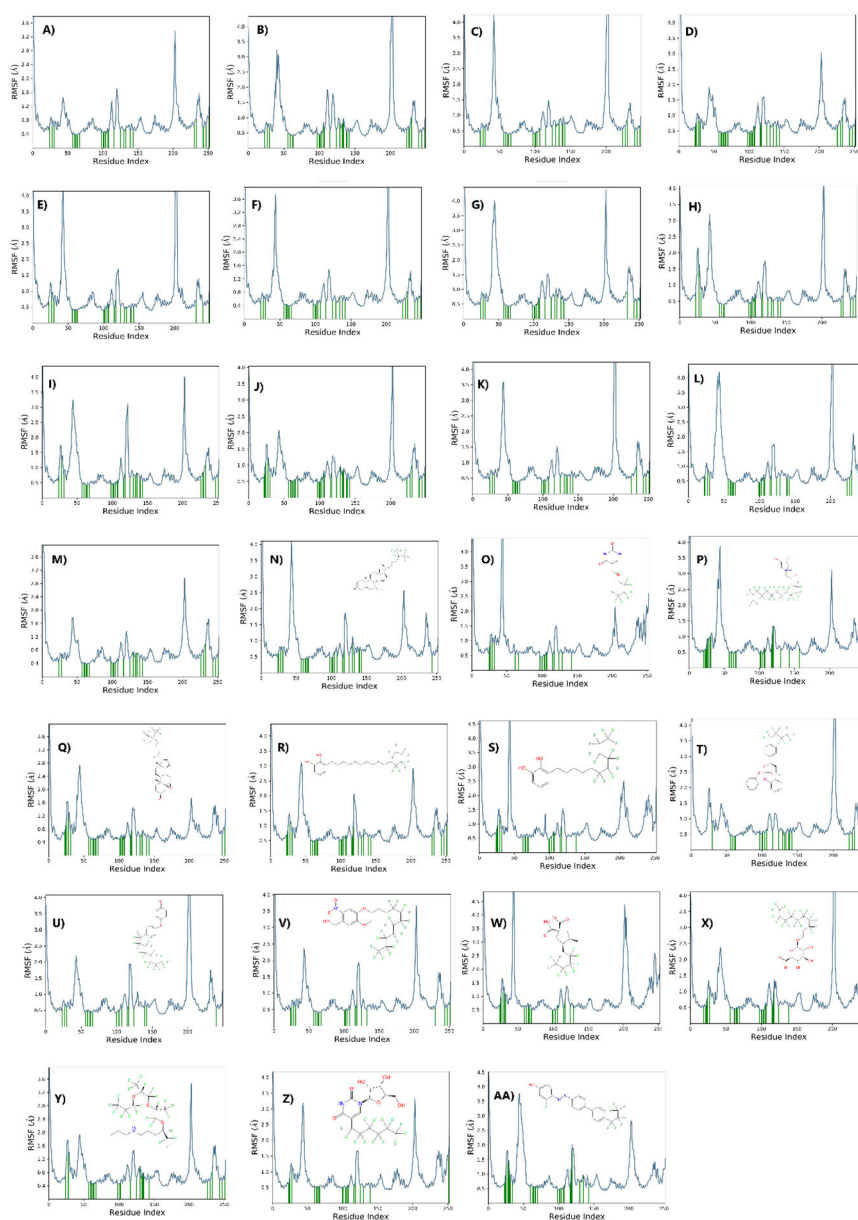
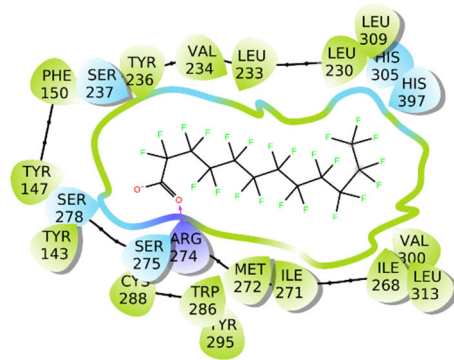
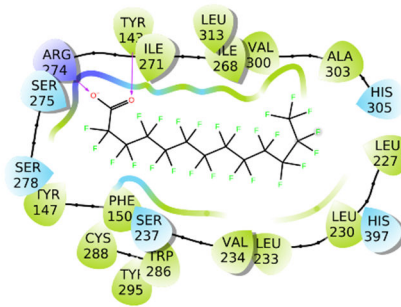


Figure 6. RMSF (\AA) of residues of VDR + known ligands and top ranking VDR+ PFAS complexes. A) Alfacalcidol B) Calcidol, C) Calcitriol, D) Eldecalcitol, E) Calciferol, F) Calcipotriol, G) Doxercalciferol, H) Ergocalciferol, I) Falcacalcitriol, J) Inecalcitol, K) Paricalcitol L) Secalcitol, M) Tacalcitol, N) DTXSID40897496, O) DTXSID30309992, P) DTXSID40881032, Q) DTXSID20897499, R) DTXSID60895974, S) DTXSID70895980 T) DTXSID80827555, U) DTXSID90896292, V) DTXSID40896227, W) DTXSID50379718, X) DTXSID50858139 Y) DTXSID10896537, Z) DTXSID90785778 and AA) DTXSID30896731 Green lines shows the residues where the ligand interacts with VDR. (Residues numbers are reset to starting at zero. See Supporting Information Table S1 for residue mapping details.)



Perfluorododecanoic acid
DTXSID8031861

$$\Delta G_{\text{bind}} = -7.934 \pm 0.686 \text{ (kcal/mol)}$$



Perfluorotridecanoic acid
DTXSID90868151

$$\Delta G_{\text{bind}} = -18.426 \pm 0.32 \text{ (kcal/mol)}$$

Figure 7.

2D diagrams of VDR interactions with two commercially important PFASs. Alchemical free energies of binding are also shown.

Table 1,

Docking scores and alchemical free energies of binding for known VDR ligands.

Name	Docking score	MM-GBSA G_{bind} (kcal/mol)	Alchemical G_{bind} (kcal/mol)
Alfacalcidol	-13.09	-74.38	-33.038±0.382
Calcidiol	-13.13	-72.90	-19.404±0.43
Calciferol	-12.44	-74.10	-27.046±0.266
Calcipotriol	-14.97	-75.05	-33.171±0.2
Calcitriol*	-14.76	-75.67	-22.204±0.161
Doxercalciferol	-12.99	-75.07	-21.042±0.257
Eldecalcitol	-13.34	-85.44	-20.188±0.544
Ergocalciferol	-11.86	-71.99	-22.282±0.412
Falecalcitriol	-16.13	-77.66	-23.458±0.506
Inecalcitol	-12.72	-67.55	-27.071±0.188
Paricalcitol	-14.43	-77.62	-19.527±0.398
Seocalcitol	-11.81	-80.99	-30.107±0.561
Tacalcitol	-15.11	-75.58	-26.386±0.329

* 1,25-dihydroxy vitamin D3, the natural ligand of VDR.

Table 2. Docking scores and free energies of binding for the top 14 PFASs with docking scores < -12.

DTXSID	CASRN	Preferred Name	Docking Score	MM-GBSA (G_{bind} (kcal/mol))	Alchemical (G_{bind} (kcal/mol))	Primary Class	Secondary Class
DTXSID40896227	855929-03-0	{4-[(4,4,5,5,6,6,7,7,8,8,9,9,10,10,11,11,11-Heptafluoroundecyl)oxy]-5-methoxy-2-nitrophenyl)methanol	-13.057	-66.2631	-25.032±0.391	Side-chain aromatics	Others
DTXSID40897496	240129-40-2	(3 β ,7 α)-25,26,26,26,27,27,27-Heptafluorocholest-5-ene-3,7-diol	-12.278	-71.9518	-22.221±0.257	Side-chain aromatics	Others
DTXSID70895980	131545-70-5	3-(6,6,7,7,8,8,9,10,10,11,11,11-Tridecafluoroundecyl)benzene-1,2-diol	-12.652	-51.8161	-21.139±0.415	Side-chain aromatics	Others
DTXSID20897499	240129-21-9	(3 β ,5 α ,6 α)-5,6-Epoxy-25,26,26,26,27,27,27-heptafluorocholestan-3-ol	-12.103	-68.2834	-21.007±0.501	Other aliphatics, cyclic	Others, cyclic
DTXSID60895974	131545-71-6	3-(12,12,13,13,14,14,15,15,15-Nonafluoropentadecyl)benzene-1,2-diol	-12.566	-64.5733	-20.922±0.178	Side-chain aromatics	Others
DTXSID30896731	113448-90-1	3-Fluoro-4-[(E)-[4-(heptafluoropropyl) [1,1'-biphenyl]-4-yl]diazanyl]phenol	-12.298	-53.187	-20.782±0.337	Side-chain aromatics	Others
DTXSID90785778	404580-53-6	4-[4-(Heptaecafluoroethyl)phenoxy]phenol	-12.929	-57.2147	-17.701±0.198	Side-chain aromatics	Others
DTXSID80827555	846543-02-0	1-[4-(Nonafluorobutyl)phenyl]butyl diphenyl phosphate	-12.142	-71.6464	-16.122±0.437	Side-chain aromatics	Others
DTXSID40881032	93776-16-0	Bis(2-hydroxyethyl)methyl(3-(perfluorododecyl)-2-hydroxypropyl)ammonium iodide	-12.142	-65.131	-9.445±0.580	Steroid-Backbone	Steroid-Backbone
DTXSID50858139	864551-34-8	3,3,4,4,5,5,6,6,7,7,8,8,9,9,10,10,10-Heptaecafluoroethyl beta-D-glucopyranosiduronic acid	-12.809	-55.4244	-3.848±0.350	Side-chain aromatics	Others
DTXSID10896537	928655-42-9	4,5,5,5-Tetrafluoro-4-[1,1,2,3,3,3-hexafluoro-2-[1,1,2,3,3,3-hexafluoro-2-(heptafluoropropoxy)propoxy]propoxy]-N-propylpentan-1-amine	-12.036	-62.4256	-3.160±0.280	Other aliphatics	Others
DTXSID50379718	20116-32-9	3-methyl-4-(2,2,3,3,4,4,5,5,5-nonafluoropentyl)cyclopentane-1,1-dicarboxylic Acid	-12.072	-44.596		Steroid-Backbone	Steroid-Backbone
DTXSID30309992	59727-25-2	5-[(2,2,3,3,4,4,4-Hepptafluorobutoxy)methyl]-2,4(1H,3H)-pyrimidinone	-12.667	-39.8814			
DTXSID90896292	58671-32-2	5-(Tridecafluoroethyl)uridine	-13.627	-53.8179			

Table 3.

Docking scores for commercially important PFASs with docking scores better than PFOA.

DTXSID	Preferred Name	CASRN	Docking score	MM-GBSA (Gbind (kcal/mol))
DTXSID8031861 *	Perfluorododecanoic acid (PFDoA)	307-55-1	-11.32	-46.24
DTXSID60880406	2H-Tricosafuoro-5,8,11,14-tetrakis(trifluoromethyl)-3,6,9,12,15-pentaoxaoctadecane	37486-69-4	-10.42	-63.59
DTXSID3068170	2-(Perfluorododecyl)ethanol	39239-77-5	-10.36	-48.69
DTXSID6070221	1,1,2,2-Tetrahydroperfluoro-1-octadecanol	65104-67-8	-10.31	-58.08
DTXSID8059922	2-(N-Ethylperfluorooctanesulfonamido)ethyl methacrylate	376-14-7	-10.15	-60.63
DTXSID5059878	Perfluorohexadecyl iodide	355-50-0	-10.051	-59.46
DTXSID7062295	N-Butylheptadecafluoro-N-(2-hydroxyethyl)octanesulphonamide	2263-09-4	-10.03	-54.82
DTXSID6027426 *	2-Perfluorooctylsulfonyl-N-ethylaminoethyl alcohol	1691-99-2	-10.02	-50.77
DTXSID6067836	1,1,2,2-Tetrahydroperfluorohexadecyl acrylate	34362-49-7	-9.93	-62.39
DTXSID40861915	2-(N-Butylperfluorooctanesulfonamido)ethyl acrylate	383-07-3	-9.86	-63.06
DTXSID4069422	2-(Perfluorotetradecyl)ethan-1-ol	60699-51-6	-9.83	-51.61
DTXSID3031860 *	Perfluorodecanoic acid (PFDA)	335-76-2	-9.75	-40.40
DTXSID3071727	(Perfluorododecyl)ethylsulfonyl chloride	68758-57-6	-9.72	-56.33
DTXSID0059798	1H,1H,11H-Eicosafuoro-1-undecanol	307-70-0	-9.70	-40.13
DTXSID5059797	Nonacosafuoro-1-iodotetradecane	307-63-1	-9.69	-51.51
DTXSID4041284	6:2 Fluorotelomer sulfonamide betaine	34455-29-3	-9.68	-61.29
DTXSID3059921 *	Perfluorotetradecanoic acid (PFTA)	376-06-7	-9.67	-50.92
DTXSID1070800	Perfluorohexadecanoic acid (PFHxDA)	67905-19-5	-9.65	-56.01
DTXSID30889183	3-Methyl-3-[[[(3,3,4,4,5,5,6,6,6-nonafluorohexyl)oxy]methyl]-oxetane	475678-78-5	-9.59	-39.87
DTXSID00880243	Fluoroether E4	26738-51-2	-9.57	-50.69
DTXSID2029905	10:2 Fluorotelomer alcohol	865-86-1	-9.57	-42.29
DTXSID9067514	Perfluorooctadecyl iodide	29809-35-6	-9.52	-64.08
DTXSID7027831 *	N-Methyl-N-(2-hydroxyethyl)perfluorooctanesulfonamide	24448-09-7	-9.50	-48.85
DTXSID90868151 *	Perfluorotridecanoic acid (PFTRDA)	72629-94-8	-9.50	-47.87
DTXSID6062204	10:2 Fluorotelomer methacrylate	2144-54-9	-9.42	-50.04
DTXSID40892507 *	Perfluoro(2-((8-chlorohexyl)oxy)ethanesulfonic acid) (6:2 Cl-PFAES)	763051-92-9	-9.38	-51.38
DTXSID1064083	3,3,4,4,5,5,6,6,7,7,8,8,9,9,10,10,11,11,12,12,13,13,14,14,14-Pentacosafuorotetradecyl methacrylate	6014-75-1	-9.31	-58.03
DTXSID1066071	Perfluorooctadecanoic acid	16517-11-6	-9.30	-61.35
DTXSID9037743	10:2 Fluorotelomer acrylate	17741-60-5	-9.28	-51.81
DTXSID4069501	N-((Perfluorooctyl)-1-ethyl)pyridinium 4-methylbenzenesulfonate	61798-68-3	-9.26	-44.08
DTXSID8031863 *	Perfluorononanoic acid (PFNA)	375-95-1	-9.25	-37.04
DTXSID1037303 *	Perfluoroheptanoic acid (PFHpA)	375-85-9	-9.24	-31.38

DTXSID	Preferred Name	CASRN	Docking score	MM-GBSA (Gbind (kcal/mol))
DTXSID5067841	1,1,2,2-Tetrahydroperfluorotetradecyl acrylate	34395-24-9	-9.22	-59.05
DTXSID1067330	3,3,4,4,5,5,6,6,7,7,8,8,9,9,10,10,11,11,12,12-Henicosafuorododecane-1-sulphonyl chloride	27619-91-6	-9.19	-50.86
DTXSID5062760*	2-(N-Ethylperfluorooctanesulfonamido)acetic acid (Et-PFOA-AcOH)	2991-50-6	-9.16	-53.93
DTXSID10897307	Europium tri[3-(heptafluoropropylhydroxymethylene)]-(+)-camphorate	34788-82-4	-9.15	-42.29
DTXSID6071665	Pentadecafluoro-N-(2-hydroxyethyl)-N-methyl-1-heptanesulfonamide	68555-76-0	-9.12	-44.86
DTXSID2067535	1-Iodo-1H,1H,2H,2H-perfluorotetradecane	30046-31-2	-9.09	-50.97
DTXSID5067348	3,3,4,4,5,5,6,6,7,7,8,8,9,9,10,10,10-Heptadecafluorodecylacrylate	27905-45-9	-9.06	-42.41
DTXSID7029904	3,3,4,4,5,5,6,6,7,7,8,8,9,9,10,10,10-Heptadecafluoro-1-decanol	678-39-7	-9.06	-35.48
DTXSID60881337	Perfluoro(4a-(cyclohexylmethyl)decahydronaphthalene)	125061-94-1	-9.04	-46.08
DTXSID8047553*	Perfluoroundecanoic acid (PFUA)	2058-94-8	-8.99	-43.56
DTXSID7070925	N-ethyl-N-[2-(phosphonoxy)ethyl]perfluorooctanesulfonamide diammonium salt	67969-69-1	-8.98	-61.55
DTXSID60880486	Potassium N-((heptadecafluorooctyl)sulphonyl)-N-propylglycinate	55910-10-6	-8.97	-52.92
DTXSID8062101	3,3,4,4,5,5,6,6,7,7,8,8,9,9,10,10,10-Heptadecafluorodecyl methacrylate	1996-88-9	-8.91	-42.39
DTXSID80892506*	Perfluoro(2-((6-chlorohexyl)oxy)ethanesulfonic acid) (9CL-PF3ONS)	756426-58-1	-8.86	-46.54
DTXSID1071664	Tridecafluoro-N-(2-hydroxyethyl)-N-methyl-1-hexanesulfonamide	68555-75-9	-8.83	-42.34
DTXSID1047029	Perfluorotetradecahydrophenanthrene	306-91-2	-8.80	-39.35
DTXSID8059974	Perfluorodecyl iodide	423-62-1	-8.79	-40.81
DTXSID3040148	Perfluorodecane sulfonic acid	335-77-3	-8.78	-46.09
DTXSID5044572	3,3,4,4,5,5,6,6,7,7,8,8,8-Tridecafluorooctanol	647-42-7	-8.77	-31.01
DTXSID0059796	Pentacosafuoro-1-iodododecane	307-60-8	-8.75	-43.67
DTXSID5059793	7:1 Fluorotelomer alcohol	307-30-2	-8.73	-30.35
DTXSID00192353*	8:2 Fluorotelomer sulfonic acid (8:2 FTS)	39108-34-4	-8.72	-47.42
DTXSID6070510	2-(N-Methylperfluorobutanesulfonamido)ethyl methacrylate	67584-59-2	-8.72	-46.66
DTXSID3069306	2-((Ethyl(pentadecafluoroheptyl)sulfonyl)amino)ethyl acrylate	59071-10-2	-8.69	-53.62
DTXSID1070513	Potassium N-ethyl-N-((pentadecafluoroheptyl)sulphonyl)glycinate	67584-62-7	-8.67	-48.74
DTXSID1062124	10:2 Fluorotelomer iodide	2043-54-1	-8.66	-41.50
DTXSID30880413	3-(Perfluorohexyl)-1,2-epoxypropane	38565-52-5	-8.63	-30.07
DTXSID1071080	2-(Methyl((pentadecafluoroheptyl)sulfonyl)amino)ethyl acrylate	68084-62-8	-8.58	-56.19
DTXSID7070505	Potassium N-ethyl-N-((tridecafluoroheptyl)sulphonyl)glycinate	67584-53-6	-8.58	-46.06
DTXSID10624392*	2-(N-Methylperfluorooctanesulfonamido)acetic acid	2355-31-9	-8.57	-50.30
DTXSID6071663	Undecafluoro-N-(2-hydroxyethyl)-N-methyl-1-pentanesulfonamide	68555-74-8	-8.56	-39.98
DTXSID2067329	3,3,4,4,5,5,6,6,7,7,8,8,9,9,10,10,10-Heptadecafluorodecane sulphonyl chloride	27619-90-5	-8.55	-42.24
DTXSID3059975	2-(N-Ethyl-N-(perfluorooctylsulfonyl)amino)ethyl acrylate	423-82-5	-8.55	-56.54
DTXSID7070509	[N-Methylperfluorohexane-1-sulfonamide]ethyl acrylate	67584-57-0	-8.54	-51.12
DTXSID4070322	2-(Perfluorotetradecyl)-1-iodoethane	65510-55-6	-8.54	-57.78

DTXSID	Preferred Name	CASRN	Docking score	MM-GBSA (Gbind (kcal/mol))
DTXSID80865199	N-Methylperfluorooctanesulfonamidoethyl acrylate	25268-77-3	-8.53	-57.98
DTXSID9038840	Perfluorohexylethyl acrylate	17527-29-6	-8.50	-34.48
DTXSID3047558	3,3,4,4,5,5,6,6,7,7,8,8,8-Tridecafluorooctyl methacrylate	2144-53-8	-8.44	-39.62
DTXSID90881345	3-[(Perfluorooctane-1-sulfonyl)amino]-N,N-dimethylpropan-1-amine N-oxide potassium	178094-69-4	-8.44	-53.31
DTXSID6062123	3,3,4,4,5,5,6,6,7,7,8,8,9,9,10,10,10-Heptadecafluoro-1-iododecane	2043-53-0	-8.36	-39.55
DTXSID80889133	Dimethyl 2-(3,3,4,4,5,5,6,6,7,7,8,8,8-tridecafluorooctyl)-1,3-propanedioate	220075-01-4	-8.36	-44.37
DTXSID5063235	2,2,3,3,4,4,5,5,6,6,7,7,8,8,8-Pentadecafluorooctyl methacrylate	3934-23-4	-8.35	-42.29
DTXSID50880410	(3-(Perfluorooctyl)sulphonylamino)propyltrimethylammonium chloride	38006-74-5	-9.122	-60.1345
DTXSID1032646*	N-Ethylperfluorooctanesulfonamide	4151-50-2	-8.18	-49.73
DTXSID0060147	Perfluorooctyl iodide	507-63-1	-8.18	-37.33
DTXSID2070504	Potassium N-ethyl-N-((undecafluoropentyl)sulphonyl)glycinate	67584-52-5	-8.16	-41.97
DTXSID0067848	2-(N-(Perfluorobutylsulfonyl)-N-methylamino)ethanol	34454-97-2	-8.16	-35.23
DTXSID9066174	Ammonium perfluorononanesulfonate	17202-41-4	-8.13	-41.71
DTXSID1068772	2-(Perfluorobutyl)ethyl acrylate	52591-27-2	-8.11	-31.01
DTXSID6067331*	6:2 Fluorotelomer sulfonic acid	27619-97-2	-8.11	-40.25
DTXSID8031865*	PFOA	335-67-1	-8.07	-34.01

* PFAS of regulatory importance that have been detected in humans